

Velocity-Tunable Magneto-Optical-Trap-Based Cold Cs Atomic Beam

30 December 2003

Prepared by

H. WANG and W. F. BUELL
Electronics and Photonics Laboratory
Laboratory Operations

Prepared for

SPACE AND MISSILE SYSTEMS CENTER
AIR FORCE SPACE COMMAND
2430 E. El Segundo Boulevard
Los Angeles Air Force Base, CA 90245

20040219 121

Engineering and Technology Group



**THE AEROSPACE
CORPORATION**

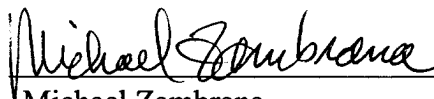
El Segundo, California

APPROVED FOR PUBLIC RELEASE;
DISTRIBUTION UNLIMITED

This report was submitted by The Aerospace Corporation, El Segundo, CA 90245-4691, under Contract No. FA8802-04-C-0001 with the Space and Missile Systems Center, 2430 E. El Segundo Blvd., Los Angeles Air Force Base, CA 90245. It was reviewed and approved for The Aerospace Corporation by B. Jaduszliwer, Principal Director, Electronics and Photonics Laboratory. Michael Zambrana was the project officer for the Mission-Oriented Investigation and Experimentation (MOIE) program.

This report has been reviewed by the Public Affairs Office (PAS) and is releasable to the National Technical Information Service (NTIS). At NTIS, it will be available to the general public, including foreign nationals.

This technical report has been reviewed and is approved for publication. Publication of this report does not constitute Air Force approval of the report's findings or conclusions. It is published only for the exchange and stimulation of ideas.

A handwritten signature in cursive script, reading "Michael Zambrana", written over a horizontal line.

Michael Zambrana
SMC/AXE

REPORT DOCUMENTATION PAGE				Form Approved OMB No. 0704-0188	
Public reporting burden for this collection of information is estimated to average 1 hour per response, including the time for reviewing instructions, searching existing data sources, gathering and maintaining the data needed, and completing and reviewing this collection of information. Send comments regarding this burden estimate or any other aspect of this collection of information, including suggestions for reducing this burden to Department of Defense, Washington Headquarters Services, Directorate for Information Operations and Reports (0704-0188), 1215 Jefferson Davis Highway, Suite 1204, Arlington, VA 22202-4302. Respondents should be aware that notwithstanding any other provision of law, no person shall be subject to any penalty for failing to comply with a collection of information if it does not display a currently valid OMB control number. PLEASE DO NOT RETURN YOUR FORM TO THE ABOVE ADDRESS.					
1. REPORT DATE (DD-MM-YYYY) 30-12-2003		2. REPORT TYPE		3. DATES COVERED (From - To)	
4. TITLE AND SUBTITLE Velocity-Tunable Magneto-Optical-Trap-Based Cold Cs Atomic Beam				5a. CONTRACT NUMBER FA8802-04-C-0001	
				5b. GRANT NUMBER	
				5c. PROGRAM ELEMENT NUMBER	
6. AUTHOR(S) H. Wang and W. F. Buell				5d. PROJECT NUMBER	
				5e. TASK NUMBER	
				5f. WORK UNIT NUMBER	
7. PERFORMING ORGANIZATION NAME(S) AND ADDRESS(ES) The Aerospace Corporation Laboratory Operations El Segundo, CA 90245-4691				8. PERFORMING ORGANIZATION REPORT NUMBER TR-2004(8555)-3	
9. SPONSORING / MONITORING AGENCY NAME(S) AND ADDRESS(ES) Space and Missile Systems Center Air Force Space Command 2450 E. El Segundo Blvd. Los Angeles Air Force Base, CA 90245				10. SPONSOR/MONITOR'S ACRONYM(S) SMC	
				11. SPONSOR/MONITOR'S REPORT NUMBER(S) SMC-TR-04-08	
12. DISTRIBUTION/AVAILABILITY STATEMENT Approved for public release; distribution unlimited.					
13. SUPPLEMENTARY NOTES					
14. ABSTRACT In this paper we report our observation and investigation of a MOT-based low-velocity Cs atomic beam for atomic clock applications. A continuous Cs atomic beam is generated from a vapor-cell magneto-optical trap (MOT) of Cs atoms by forming a leak tunnel along one of the trapping laser beams. The mean velocity of the cold Cs beam is measured by the time of flight (TOF) technique to be 7.3 m/s with a velocity spread of 1 m/s under nominal experimental conditions. By adjusting the MOT parameters, we are able to tune the Cs-beam velocity from 5 m/s to 8.5 m/s while the velocity spread remains to be 1 m/s. The Cs beam has an instantaneous atomic flux of 3.6×10^{10} atoms/s when operated in pulsed mode and an estimated continuous beam flux of 2×10^8 atoms/s. The acceleration kinetics of the Cs beam in the acceleration region is analyzed and simulated. Our theoretical model reveals that the MOT inhomogeneous magnetic field and the varying Doppler shift along the atomic beam propagation play an important role in determining the final velocity of the Cs atomic beam. Our numerical results of the atomic beam velocity on MOT parameters agree well with the measurements.					
15. SUBJECT TERMS Atomic clock, Cooling and trapping, Atomic beam					
16. SECURITY CLASSIFICATION OF:			17. LIMITATION OF ABSTRACT	18. NUMBER OF PAGES 6	19a. NAME OF RESPONSIBLE PERSON He Wang
a. REPORT UNCLASSIFIED	b. ABSTRACT UNCLASSIFIED	c. THIS PAGE UNCLASSIFIED			19b. TELEPHONE NUMBER (include area code) (310)336-5863

Note

The material reproduced in this report originally appeared in *Journal of the Optical Society of America B*. The TR is published to document the work for the corporate record.

He Wang and Walter F. Buell, "Velocity-tunable magneto-optical-trap-based cold Cs atomic beam," *Journal of Optical Society of America B*, Vol. 20, No. 10, October 2003.

Contents

1. Introduction	1
2. Experiment and Results	2
3. Analysis	4
4. Conclusions	6
References	6

Figures

1. Two-dimensional schematic diagram of the formation of the MOT-based Cs atomic beam	2
2. Laser-induced fluorescence image of the MOT-based continuous Cs atomic beam	2
3. TOF measurement of the Cs atomic beam velocity	3
4. TOF measurements of the MOT-based Cs beam velocity as a function of the MOT magnetic field gradient and the acceleration laser frequency.....	3
5. Schematic diagram of the acceleration region of the MOT-based Cs atomic beam	3
6. Theoretical simulation of the MOT-based Cs atomic beam	5

PRECEDING PAGE BLANK

Velocity-tunable magneto-optical-trap-based cold Cs atomic beam

He Wang and Walter F. Buell

Electronics and Photonics Laboratory, The Aerospace Corporation, P.O. Box 92957, M2-253, Los Angeles, California 90009-2957

Received January 20, 2003; revised manuscript received June 2, 2003

We report our observation and investigation of a magneto-optical-trap- (MOT)-based low-velocity Cs atomic beam for atomic clock applications. We generated a continuous Cs atomic beam from a vapor-cell MOT of Cs atoms by forming a leak tunnel along one of the trapping laser beams. The mean velocity of the cold Cs beam is measured by the time-of-flight technique to be 7.3 m/s with a velocity spread of 1 m/s under nominal experimental conditions. By adjusting the MOT parameters, we are able to tune the Cs beam velocity from 5 to 8.5 m/s while the velocity spread remains at 1 m/s. The Cs beam has an instantaneous atomic flux of 3.6×10^{10} atoms/s when operated in pulsed mode and an estimated continuous beam flux of 2×10^8 atoms/s. The acceleration kinetics of the Cs beam in the acceleration region is analyzed and simulated. Our theoretical model reveals that the MOT inhomogeneous magnetic field and the varying Doppler shift along the atomic beam propagation play an important role in the determination of the final velocity of the Cs atomic beam. Our numerical results of the atomic beam velocity on MOT parameters agree well with the measurements.

© 2003 Optical Society of America

OCIS codes: 140.3320, 020.7010

1. INTRODUCTION

Laser-cooled low-velocity ($v \sim 10$ m/s) atomic beams are important in the development of space-qualified, compact, and highly stable atomic clocks because the microgravity conditions in space do not support use of atomic fountains.^{1–5} For example, when a beam of Cs atoms is used at a velocity of 10 m/s, the clock interrogation time could be increased by approximately 15–25 times compared with the commercial Cs beam atomic clocks operating at thermal beam velocities of ~ 150 –250 m/s.⁶ With the laser cooling and trapping technique, one can generate a cold atomic beam by directly laser decelerating a thermal atomic beam or by laser accelerating an ensemble of ultracold ($T < 1$ mK) atoms from a laser-cooled atomic trap. The former usually requires a spatial distance of ~ 1 m to cool a beam of alkali atoms to the expected velocities,^{5,7,8} which defines the dimensions of the instrument. However, the latter technique has the unique advantage of generating a useful low-velocity atomic beam just outside the volume of an atomic trap, for example, a vapor-cell magneto-optical trap (MOT), and hence greatly improves the system compactness. MOT-based low-velocity Rb and Cs atomic beams have recently been reported.^{9–11} The basic idea of this method is to introduce a controlled leak to a MOT by a modification of the trapping potential so that the MOT functions like a cold atom funnel, with which thermal atoms are captured, cooled, and then pushed out to form an atomic beam. Because the atomic beam thus formed originates from an ensemble of cold atoms at ~ 100 μ K, one can obtain low beam velocities by controlling the laser acceleration process. Two techniques have been reported for the implementation of such a low-velocity atomic beam. Lu *et al.*⁹ use a specially fabricated mirror with a small hole at the

center to form a hollowed retroreflected trapping beam in a Rb MOT. Rb atoms are then pushed out of the MOT by the trapping laser beam propagating toward the mirror and travel through the hole to become a Rb atomic beam. The one laser beam conical or pyramidal mirror MOT configuration has also been adapted to generate cold Rb and Cs atomic beams based on the same idea.^{10–11} If a small hole is fabricated at the apex of the pyramid or conical mirror, cold atoms trapped in the one-beam MOT can leak out through the hole to form an atomic beam. The advantage of this method is system simplicity because only one cooling and trapping laser beam is needed for the MOT.⁴ However, the atomic beam generated by the one-beam MOT configuration is under constant acceleration even after the atoms have left the MOT region. This is because the trapping laser beam and the optical repumping laser beam for the one-beam MOT cannot be separated, and the atomic beam copropagates and interacts with both of them through the hole in the pyramid or conical mirror. For the above two methods, specially fabricated optical mirrors are required and have to be installed inside the vacuum chamber, which is loaded with relatively dense alkali metal vapors.

In this paper we report our observation and investigation of a low-velocity Cs atomic beam generated from a regular vapor-cell Cs MOT. In our system, no specially fabricated optics are used inside the vacuum chamber. We separate the optical repumping laser beam from the trapping laser beam that is responsible for accelerating the cold Cs atoms and in fact use the MOT repumping laser beam to define a controllable acceleration region near the MOT volume. In this way the Cs beam travels at an approximately uniform velocity after leaving the vicinity of the trap volume. In Section 2 we report our experi-

ments on the generation of the MOT-based Cs atomic beam and the time-of-flight (TOF) measurement of the Cs beam velocities. In Section 3 we present our nonlinear theoretical model that describes and simulates the acceleration kinetics of the MOT-based Cs atomic beam. In Section 4 we summarize our results and briefly discuss the prospects for atomic clock applications using the cold continuous Cs atomic beam.

2. EXPERIMENT AND RESULTS

The low-velocity Cs atomic beam is generated from a vapor-cell MOT of Cs atoms. Briefly, our Cs MOT traps 8×10^7 atoms with a density of 8×10^{10} atoms/cm³ at ~ 300 μ K. The Cs trap has a loading time constant of 0.4 s. The MOT is accommodated in an ultrahigh vacuum chamber with a background pressure of 6×10^{-10} Torr. The windows of the vacuum chamber are coated with broadband near-IR antireflection coatings. Two 150-mW distributed Bragg reflection diode lasers (SDL-5722-H1) at 852 nm are used for the cooling and trapping and the optical repumping. The diode laser temperature is regulated with an ILX Lightwave LDT-5910B temperature controller for stable operation at 852 nm. The single-mode distributed Bragg reflection laser has an effective linewidth of ~ 3 MHz, and the laser frequency is actively stabilized with a saturated absorption spectrometer for long-term frequency stability. Specifically, the trapping laser is locked to the crossover saturated absorption line (125 MHz below the highest $F' = 5$ level) between the transitions $6^2S_{1/2}(F'' = 4) \rightarrow 6^2P_{3/2}(F' = 5)$ and $6^2S_{1/2}(F'' = 4) \rightarrow 6^2P_{3/2}(F'' = 4)$. The optical repumping laser is stabilized to the $6^2S_{1/2}F'' = 3 \rightarrow 6^2P_{3/2}F' = 4$ transition. The trapping laser frequency, after it is upshifted by 100 MHz with an acousto-optical modulator (IntraAction ATM-1001A2), is 25-MHz red detuned from the $6^2P_{3/2}F' = 5$ hyperfine level. We can adjust this red detuning by tuning the rf of the acousto-optic modulator driver (IntraAction VFE-1102A4).

Figure 1 is a two-dimensional schematic diagram that shows the generation of the Cs beam from the Cs MOT. We perturb the MOT trapping potential by making one of the six trapping laser beams into a hollowed laser beam in the traveling direction of the Cs beam. We create the hollowed trapping beam by blocking the center part of the well-collimated laser beam with a round opaque spot on the surface of an antireflection-coated glass disk located outside the vacuum chamber at a distance of 30 cm from the Cs MOT. The small opaque spot has a diameter of ~ 1 mm for a trapping laser beam cross section of 18 mm in diameter. This configuration makes a controlled leak tunnel off the atomic trap along the hollowed trapping laser beam while the MOT captures and cools the Cs atoms from the surrounding Cs vapor. We introduce the MOT optical repumping beam (not shown in Fig. 1 but shown in Fig. 5) by overlapping it only with the vertical trapping beams that are perpendicular to the Cs atomic beam.

Once the leak tunnel is formed, the balance of the force that confines atoms in the trap breaks down, and the trapped Cs atoms experience a net spontaneous force from the acceleration laser beam, that is, the trapping laser beam propagating in the opposite direction of the hol-

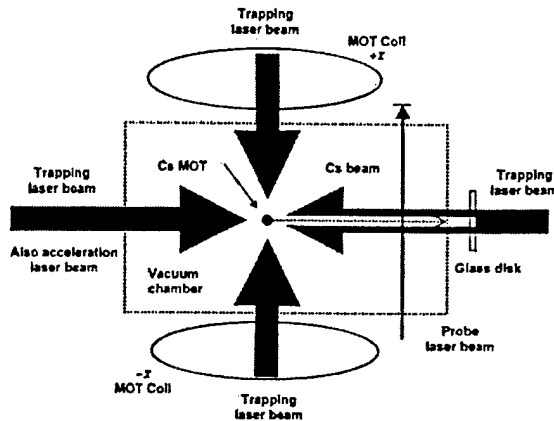


Fig. 1. Two-dimensional schematic diagram of the formation of a MOT-based Cs atomic beam. For clarity, only four MOT laser beams are shown. The dotted line indicates that the glass disk, which creates the hollowed trapping beam, is located outside the vacuum chamber. The hollowed dark column has a cross section of ~ 1 mm in diameter whereas the trapping laser beam is 18 mm in diameter.

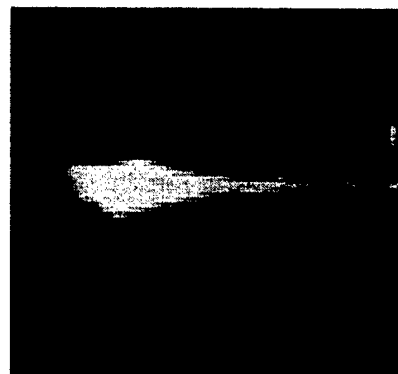


Fig. 2. Laser-induced fluorescence image of the MOT-based continuous Cs atomic beam. The bright spot is the trapped cold Cs atomic cloud, and the relatively weaker narrow line is the Cs atomic beam traveling to the right.

lowed trapping beam as shown in Fig. 1. The spontaneous force (radiation pressure force) can be described by⁷

$$F_{sp} = \frac{\hbar k S_0 \gamma / 2}{1 + S_0 + (2\delta/\gamma)^2}, \quad (1)$$

where $\hbar k$ is the photon momentum, γ is the natural linewidth of the atomic transition, and δ is the off-resonance detuning of the acceleration laser (the trapping laser). $S_0 = I/I_s$ stands for the saturation parameter where I and I_s are the acceleration laser intensity and the saturation intensity for the atomic transition, respectively. A continuous Cs atomic beam is observed and imaged by laser-induced fluorescence as shown in Fig. 2. The bright spot is the trapped Cs cloud, and the Cs beam can be seen to the right of the trap. This image shows the Cs atomic beam formed from the MOT, and the fluorescence is induced by the trapping and the optical repumping laser beams. Note that Fig. 2 is a snapshot of a continuous operation of the MOT-based Cs atomic beam. To clearly

show both the MOT cloud and the atomic beam, we controlled the MOT leak rate to be low by using an opaque spot of ~ 0.5 mm in diameter, about half of the size of the Cs trap volume.

The mean velocity of the MOT-based Cs beam is measured by the TOF method. To perform the TOF measurement, we operate the MOT beam system in a semicontinuous mode with the trapped Cs atomic cloud launched from the MOT repeatedly at a rate of 1 Hz. A probe laser beam, focused to approximately 1 mm in diameter, crosses the atomic beam at a distance of 11 cm downstream from the MOT. This probe beam is part of the MOT repumping laser beam whose frequency is locked to the $6^2S_{1/2} F' = 3 \rightarrow 6^2P_{3/2} F' = 4$ transition. As the Cs atoms pass through the probe beam, laser-induced fluorescence is recorded with a photomultiplier tube in a direction perpendicular to both the atomic beam and the probe laser beam. Figure 3 demonstrates a typical TOF signal for the measurement. The horizontal axis is the time the Cs atoms take to travel through a distance of 11 cm from the MOT center to the probe laser beam. The Cs atoms start leaving the MOT volume at $t = 0$. As shown in Fig. 3, this measurement records a flight time of 15.1 ms, giving an averaged beam mean velocity of 7.3 m/s under typical experimental conditions. Note that the Cs atoms gain their full speed only in a short acceleration distance less than 10% of the total flight path and travel without further acceleration during most of their flight time. A detailed analysis and simulation of the acceleration process are presented in Section 3. The linewidth (FWHM) of the TOF signal as shown in Fig. 3 is 2.2 ms, indicating an atomic beam velocity spread of 1 m/s. This velocity spread is mainly due to the initial spatial and momentum distribution of the Cs atoms in the MOT volume ($V \sim 1 \text{ mm}^3$ and $T \sim 300 \mu\text{K}$). Assuming that all the 8×10^7 trapped Cs atoms pass through the probe laser beam in 2.2 ms, we obtain a pulsed beam flux of 3.6×10^{10} atoms/s. We estimate a continuous Cs beam flux of 2×10^8 atoms/s from the measured MOT loading rate.

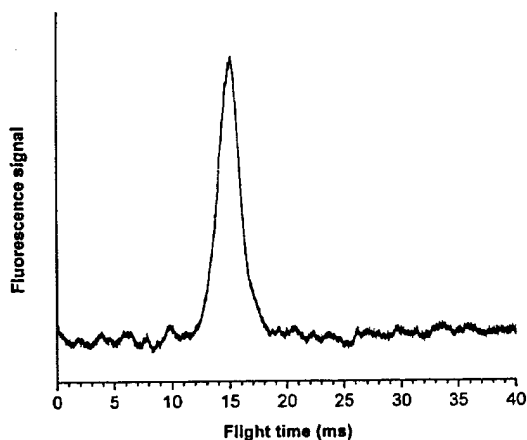


Fig. 3. TOF measurement of the Cs atomic beam velocity. Laser-induced fluorescence is recorded at 11 cm downstream from the MOT when the system is operated in a semicontinuous mode. The peak flight time gives a mean beam velocity of 7.3 m/s, and the width (FWHM) of the signal indicates a velocity spread of 1 m/s.

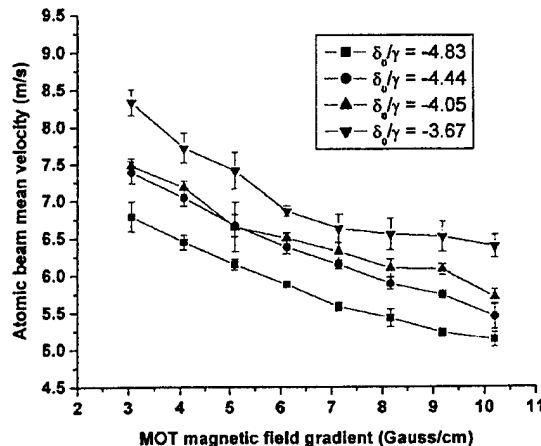


Fig. 4. TOF measurements of the MOT-based Cs beam velocity as a function of the MOT magnetic field gradient and the acceleration laser frequency. The error bars are 1 standard deviation of the statistical uncertainty of the measured atomic beam mean velocity.

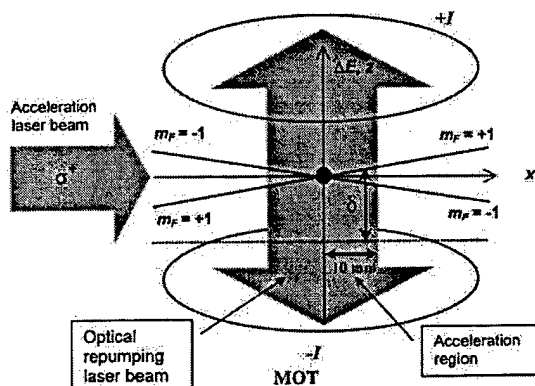


Fig. 5. Schematic diagram of the acceleration region of the MOT-based Cs atomic beam. The x axis is the direction in which the Cs beam travels. The solid dot at $x = 0, z = 0$ represents the trapped Cs atomic cloud before it is pushed out. The MOT anti-Helmholtz coils generate an approximately constant magnetic field gradient $\partial B/\partial x$ along the x axis in the vicinity of the MOT center. The two crossed lines, labeled $m_F = +1$ and $m_F = -1$, represent the simplified atomic hyperfine levels shifted by the Zeeman effects. The vertical axis also stands for the relative energy ΔE to the atomic resonance, and the horizontal dotted line with $\Delta E < 0$ indicates the red-detuned acceleration laser frequency. Both the acceleration laser beam and the optical repumping laser beam are circularly polarized. δ is the total off-resonance detuning of the acceleration laser.

Our experimental tests show that the Cs atomic beam velocity varies as a function of several MOT parameters. Using the TOF technique, we were able to measure the velocity dependence on the acceleration laser frequency and intensity as well as the MOT magnetic field gradients. Figure 4 shows the measured Cs beam velocity as a function of the MOT magnetic field gradient. The four sets of data correspond to four different frequencies that were set for the acceleration laser. Note that the acceleration laser beam is one of the trapping laser beams, and its frequency is red detuned from resonance by a few

times the natural linewidth γ . From the measurements we found that the Cs beam velocity decreases as the magnetic field gradient increases. This is because the Zeeman effects from the inhomogeneous magnetic field increase the total off-resonance detuning of the acceleration laser, resulting in a reduced spontaneous force as indicated in Eq. (1) and as designated in Fig. 5. Similarly, a larger red detuning, δ_0/γ , reduces the velocity of the Cs beam. Here $\delta_0 = \nu_L - \nu_0$ is the red detuning of the acceleration laser, and ν_L and ν_0 are the laser frequency and the atomic resonance frequency, respectively. The FWHM linewidth γ of the relevant Cs atomic transition equals 5.18 MHz. The error bars in Fig. 4 are 1 standard deviation of the statistical uncertainty of the measured atomic beam mean velocity. The largest error bar in Fig. 4 is 0.5 m/s, approximately half of the thermal mean velocity spread (1 m/s) as given by the width of the TOF signal. As can be seen in Fig. 4, we can tune the Cs atomic beam velocity to a range of 5–8.5 m/s with a velocity spread of 1 m/s by adjusting the MOT parameters. The ability to control the atomic beam velocity may be useful for the implementation of a highly stable atomic beam by means of actively stabilizing the beam velocity. In addition, we also measured the relationship between the Cs beam velocity and the acceleration laser intensity as shown in Fig. 6(d).

3. ANALYSIS

As described above, the Cs atomic beam is generated from an ultracold source, the Cs MOT, where Cs atoms have thermal temperatures of $\sim 300 \mu\text{K}$. This ultralow temperature corresponds to a thermal mean velocity of $\sim 20 \text{ cm/s}$ for Cs atoms. In the theoretical model developed below, we ignore the initial thermal velocity of the cold atoms and consider only the longitudinal motion of the Cs atomic beam. From Eq. (1), the spontaneous force F_{sp} gives the Cs atoms an acceleration

$$a = \frac{F_{\text{sp}}}{m_{\text{Cs}}} = \frac{\hbar k S_0 \gamma / 2m_{\text{Cs}}}{1 + S_0 + (2\delta/\gamma)^2} \quad (2)$$

Figure 5 schematically shows the region near the MOT volume where the Cs atomic beam gains its speed. Here only the acceleration laser beam and the optical repumping laser beam are shown.

The optical repumping laser beam propagates perpendicularly to the acceleration laser beam and has a beam diameter of 20 mm. For MOT operation, the optical repumping beam (its frequency is locked to the $6^2S_{1/2} F'' = 3 \rightarrow 6^2P_{3/2} F' = 4$ transition) maintains a continuous cooling and trapping process by optically pumping Cs atoms back to the $F'' = 4$ state. Because the same atomic transition schemes are used to form the atomic beam, this repumping laser beam defines an acceleration region in which Cs atoms absorb photons and are accelerated. As designated in Fig. 5, this acceleration region has an effective linear distance of 10 mm. Once the Cs atoms move out of this region they are instantly pumped by the acceleration laser into the lower $F'' = 3$ level and no longer absorb photons, causing the acceleration process to stop.

The Cs beam then travels at an approximately uniform velocity toward the probing laser beam.

Because the acceleration laser beam is circularly polarized (σ^+), it interacts only with Cs atoms in the $m_F = +1$ level in the acceleration region. In the vicinity of the MOT volume, the Zeeman shift increases approximately linearly as Cs atoms move out of the MOT volume. As the Cs atoms gain their speed, the Doppler shift also adds to the effective off-resonance detuning (the Cs beam travels in the same direction as the acceleration laser beam). We therefore obtain the total off-resonance detuning for Eq. (2):

$$\delta = \delta_0 + \mu B_x / \hbar + \Delta \nu_D, \quad (3)$$

$$\delta_0 = \nu_L - \nu_0, \quad B_x = (\partial B / \partial x)x,$$

$$\Delta \nu_D = (v/c)\nu_0, \quad (4)$$

where δ_0 is the fixed detuning of the acceleration laser and $\mu = \mu_0$ is the Bohr magnetic constant for the relevant atomic transition. The magnetic field gradient $\partial B / \partial x$ is a parameter set by the MOT coil current. $\Delta \nu_D$ stands for the Doppler shift at velocity v , and $\nu_0 = 351725718.50 \text{ MHz}$ is the Cs D_2 line resonance frequency.¹² Substituting Eqs. (3) and (4) into Eq. (2), we obtain

$$a = \frac{a_0 S_0}{1 + S_0 + \left[\frac{2}{\gamma} \left(\delta_0 + \frac{\mu}{\hbar} \frac{\partial B}{\partial x} x + \frac{\nu_0}{c} v \right) \right]^2}, \quad (5)$$

where $a_0 = \hbar k \gamma / 2m_{\text{Cs}}$ is a constant determined by the Cs mass and the photon energy. Obviously a varies as the Cs atoms travel along the x axis.

In a similar way, the optical repumping laser also becomes off resonant by $\delta' = \mu B_x / \hbar$, $B_x = (\partial B / \partial x)x$ because of the Zeeman effects once the Cs atoms leave the MOT volume. However, Doppler effects can be ignored as the repumping laser beam propagates perpendicularly to the Cs atomic beam. Therefore the optical repumping becomes less efficient as the Cs atoms travel in the x direction. This effect is incorporated into the model when we multiply Eq. (5) with a Lorentzian function. When we write $a = d^2x/dt^2$ and $v = dx/dt$, Eq. (5) becomes

$$\begin{aligned} \frac{d^2x}{dt^2} = & \frac{a_0 S_0}{1 + S_0 + \left[\frac{2}{\gamma} \left(\delta_0 + \frac{\mu}{\hbar} \frac{\partial B}{\partial x} x + \frac{\nu_0}{c} \frac{dx}{dt} \right) \right]^2} \\ & \times \frac{a' S_0'}{1 + S_0' + \left(\frac{2}{\gamma} \frac{\mu}{\hbar} \frac{\partial B}{\partial x} x \right)^2}, \end{aligned} \quad (6)$$

where $S_0' = I_{\text{repump}}/I_s$ is the saturation factor for the optical repumping laser beam and a' is a proportional constant. This nonlinear second-order differential equation describes the kinetics of the Cs atomic beam in the acceleration region shown in Fig. 5. The initial values for Eq. (6) are $x = 0$ and $dx/dt = 0$ at $t = 0$.

Equation (6) is solved numerically under the given initial conditions by use of the Mathcad differential equation solver (Mathcad 2000 Professional, MathSoft, Inc.). The results are plotted in Fig. 6 and compared with the mea-

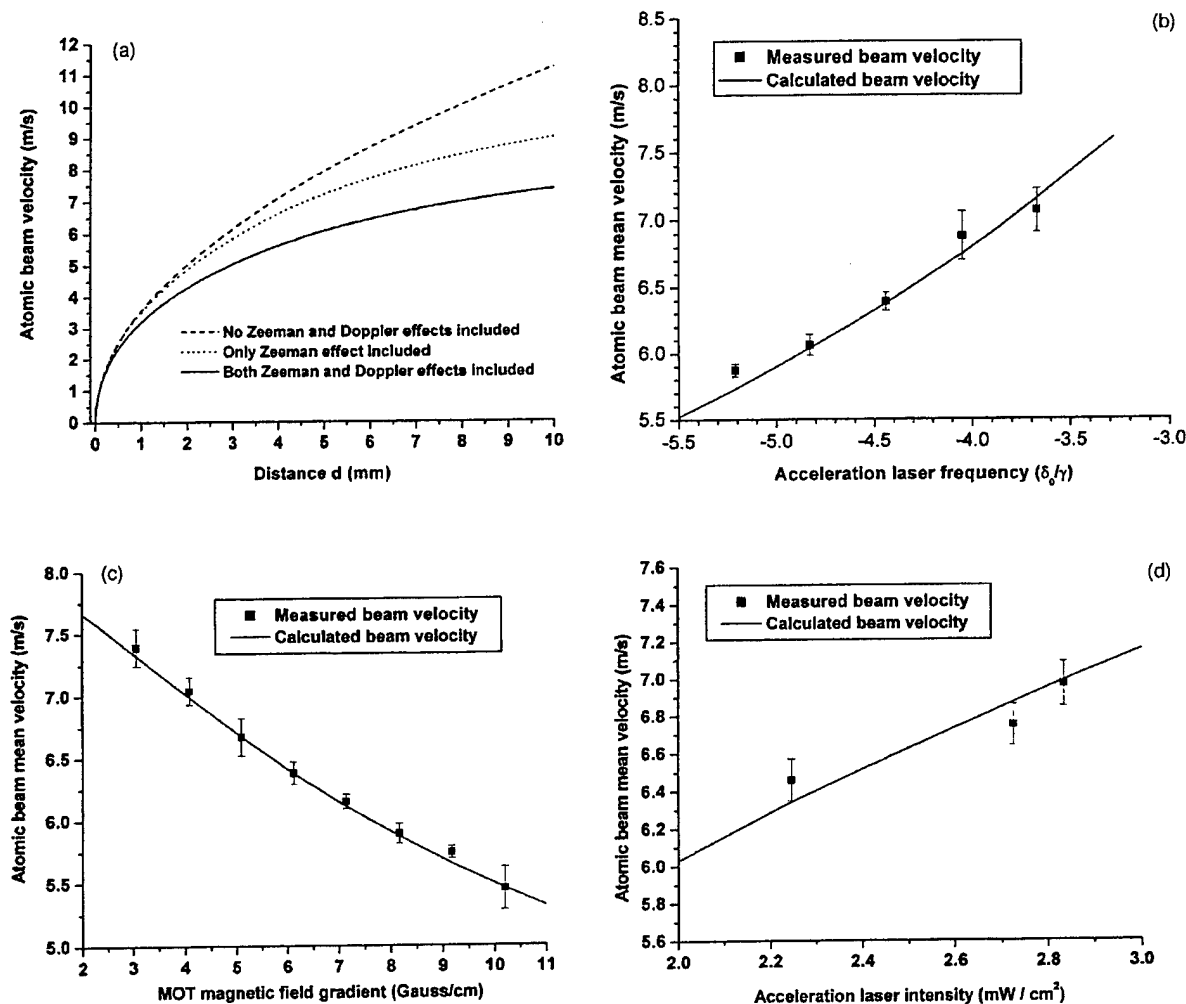


Fig. 6. Theoretical simulation of the MOT-based Cs atomic beam. (a) Presents the calculated Cs beam velocity as a function of the distance from the MOT in the acceleration region. (b) Shows the calculated and measured Cs beam mean velocity as a function of the acceleration laser frequency. Here the magnetic field gradient is 5.1 G/cm and the acceleration laser intensity is $2.8 \text{ mW}/\text{cm}^2$. (c) Compares the simulated Cs beam mean velocity with the measured values as the MOT magnetic field gradient increases. The acceleration laser has a red detuning of $\delta_0 = -4.44\gamma$. (d) Shows the velocity dependence on the acceleration laser intensity with a MOT magnetic field gradient of 4.1 G/cm and a laser frequency red detuning of $\delta_0 = -4.44\gamma$.

measurements. Figure 6(a) shows the calculated Cs beam velocity as a function of x , the distance from the MOT. The solid curve simulates the acceleration process under typical experimental conditions. At $x = 10 \text{ mm}$, where the acceleration ends, the Cs beam has gained a velocity of 7.4 m/s, which agrees with the measurement. It takes only 2 ms for the Cs atoms to travel through the 10-mm acceleration region. As the effective red detuning of the acceleration laser increases along the x axis because of the Zeeman and Doppler effects, the acceleration a reduces to approximately 20% of its maximum value at $x = 10 \text{ mm}$. The simulation indicates a much faster acceleration if the Zeeman and Doppler effects are not considered, and the atoms could gain a velocity of 11 m/s as shown by the dashed curve. This apparently disagrees with the experiment. We obtained the dotted curve in Fig. 6(a) by including the Zeeman shift but not the Doppler shift, giving a final velocity of 9 m/s, also higher than the observed value.

The strong effects of the Zeeman and Doppler shifts on the acceleration can be readily understood when we compare the magnitude of the three parts of the frequency detunings in Eq. (3). The laser red detuning $\delta_0 = -23 \text{ MHz}$ is fixed. At $x = 10 \text{ mm}$, the Zeeman shift increases to 5.7 MHz with a magnetic field gradient of 4.1 G/cm (under the approximation of a constant magnetic field gradient). Furthermore, the varying Zeeman shift appears twice in the differential equation of Eq. (6), approximately doubling its effects. On the other hand, the Cs atoms gain a Doppler shift of 8.7 MHz at a velocity of 7.4 m/s, which is not negligible compared with the 23-MHz fixed detuning. In Figure 6(b)–6(d) we compare the calculated Cs beam mean velocities with the measured values with good agreements between the theory and the experiment. We attribute the good agreement shown in Fig. 6 to the fact that we explicitly took into account the varying Zeeman and Doppler effects in the acceleration region. Our theoretical model reveals that the MOT

magnetic field affects the Cs beam acceleration by increasing the off-resonance detunings for both the acceleration and the optical repumping laser. In fact, the calculated velocity dependence has a much smaller changing rate if the Zeeman effect is not considered for the optical repumping process. It is straightforward to understand Fig. 6(b) and 6(d) where the Cs beam velocity increases as the acceleration laser has smaller red detuning and higher intensity.

4. CONCLUSIONS

In conclusion, we have demonstrated a cold Cs atomic beam produced from a MOT of Cs atoms. We have measured the Cs atomic beam mean velocity to be 7.3 m/s with a velocity spread of 1 m/s. The dependence of the atomic beam velocity on the MOT parameters has been experimentally studied. By adjusting the MOT parameters, we are able to tune the atomic beam velocity in a range of 5–8.5 m/s with a velocity spread of 1 m/s. We have also developed a nonlinear theoretical model of the spontaneous force that is responsible for the acceleration of the MOT-based Cs beam. Our calculation reveals that the inhomogeneous MOT magnetic field and the varying Doppler shift in the acceleration region have strong effects on the atomic beam final speed. This MOT-based cold Cs beam is being used to develop a compact Cs beam atomic clock.^{4,13,14} With a Ramsey separated-field microwave cavity of 20 cm long and the given Cs atomic beam parameters, we estimate that the atomic clock will have an Allen standard deviation $\sigma_y(\tau) = 1.8 \times 10^{-13} \tau^{-1/2}$ (τ is in seconds) for the short-time frequency stability under the shot-noise approximation.^{4,6,13–15} Here τ is the averaging time used to measure the clock frequency stability.

The authors thank J. C. Camparo and B. Jaduszliwer for helpful discussions and G. H. Iyanu for technical assistance. This research was supported by U.S. Air Force Space and Missile Systems Center under contract F040701-00-C-0009.

REFERENCES

1. Ph. Laurent, P. Lemonde, E. Simon, G. Santarelli, A. Clairon, N. Dimarcq, P. Petit, C. Audoin, and C. Salomon, "A cold atom clock in the absence of gravity," *Eur. Phys. J. D* **3**, 201–204 (1998).
2. T. P. Heavner, L. Hollberg, S. R. Jefferts, J. Kitching, W. M. Klipstein, D. M. Meekhof, and H. G. Robinson, "Characterization of a cold cesium source for PARCS: primary atomic reference clock in space," in *Proceedings of 2000 IEEE International Frequency Control Symposium* (Institute of Electrical and Electronics Engineers, New York, 2002), pp. 656–658.
3. C. Fertig, K. Gibble, W. M. Klipstein, L. Maleki, D. Seidel, and R. Thompson, "RACE: laser-cooled Rb microgravity clock," in *Proceedings of 2000 IEEE International Frequency Control Symposium* (Institute of Electrical and Electronics Engineers, New York, 2002), pp. 676–679.
4. W. F. Buell, "Laser-pumped and laser-cooled atomic clocks for space applications," *Laser Part. Beams* **16**, 627–639 (1998).
5. H. S. Lee, S. E. Park, T. Y. Kwon, S. H. Yang, and H. Cho, "Toward a cesium frequency standard based on a continuous slow atomic beam: preliminary results," *IEEE Trans. Instrum. Meas.* **50**, 531–534 (2001).
6. F. G. Major, *The Quantum Beat: The Physical Principles of Atomic Clocks* (Springer-Verlag, New York, 1998).
7. H. J. Metcalf and P. van der Straten, *Laser Cooling and Trapping* (Springer-Verlag, New York, 1999).
8. E. Riis, D. S. Weiss, K. A. Moler, and S. Chu, "Atom funnel for the production of a slow, high-density atomic beam," *Phys. Rev. Lett.* **64**, 1658–1661 (1990).
9. Z. T. Lu, K. L. Corwin, M. J. Renn, M. H. Anderson, E. A. Cornell, and C. E. Wieman, "Low-velocity intense source of atoms from a magneto-optical trap," *Phys. Rev. Lett.* **77**, 3331–3334 (1996).
10. K. H. Kim, K. I. Lee, H. R. Noh, and W. Jhe, "Cold atomic beam produced by a conical mirror funnel," *Phys. Rev. A* **64**, 013402 (2001).
11. A. Camposeo, A. Piombini, F. Cervelli, F. Tantussi, F. Fuso, and E. Arimondo, "A cold cesium atomic beam produced out of a pyramidal funnel," *Opt. Commun.* **200**, 231–239 (2001).
12. Th. Udem, J. Reichert, T. W. Hansch, and M. Kourogi, "Absolute optical frequency measurement of the cesium D₂ line," *Phys. Rev. A* **62**, 031801(R) (2000).
13. H. Wang and W. F. Buell, "Development of a MOT-based continuous cold Cs-beam atomic clock," Postconference Digest, in *Quantum Electronics and Laser Science*, Vol. 74, OSA Trends in Optics and Photonics (Optical Society of America, Washington D.C., 2002), pp. 93–94.
14. W. F. Buell and H. Wang, "A compact, continuous beam cold atom clock for satellite applications," in *Proceedings of the 33rd Annual Precise Time and Time Interval (PTTI) Systems and Applications Meeting* (U.S. Naval Observatory, Washington, D.C., 2002), pp. 33–43.
15. J. Vanier and L. Bernier, "On the signal-to-noise ratio and short-term stability of passive rubidium frequency standards," *IEEE Trans. Instrum. Meas.* **IM-30**, 277–282 (1981).

LABORATORY OPERATIONS

The Aerospace Corporation functions as an "architect-engineer" for national security programs, specializing in advanced military space systems. The Corporation's Laboratory Operations supports the effective and timely development and operation of national security systems through scientific research and the application of advanced technology. Vital to the success of the Corporation is the technical staff's wide-ranging expertise and its ability to stay abreast of new technological developments and program support issues associated with rapidly evolving space systems. Contributing capabilities are provided by these individual organizations:

Electronics and Photonics Laboratory: Microelectronics, VLSI reliability, failure analysis, solid-state device physics, compound semiconductors, radiation effects, infrared and CCD detector devices, data storage and display technologies; lasers and electro-optics, solid-state laser design, micro-optics, optical communications, and fiber-optic sensors; atomic frequency standards, applied laser spectroscopy, laser chemistry, atmospheric propagation and beam control, LIDAR/LADAR remote sensing; solar cell and array testing and evaluation, battery electrochemistry, battery testing and evaluation.

Space Materials Laboratory: Evaluation and characterizations of new materials and processing techniques: metals, alloys, ceramics, polymers, thin films, and composites; development of advanced deposition processes; nondestructive evaluation, component failure analysis and reliability; structural mechanics, fracture mechanics, and stress corrosion; analysis and evaluation of materials at cryogenic and elevated temperatures; launch vehicle fluid mechanics, heat transfer and flight dynamics; aerothermodynamics; chemical and electric propulsion; environmental chemistry; combustion processes; space environment effects on materials, hardening and vulnerability assessment; contamination, thermal and structural control; lubrication and surface phenomena. Microelectromechanical systems (MEMS) for space applications; laser micromachining; laser-surface physical and chemical interactions; micropropulsion; micro- and nanosatellite mission analysis; intelligent microinstruments for monitoring space and launch system environments.

Space Science Applications Laboratory: Magnetospheric, auroral and cosmic-ray physics, wave-particle interactions, magnetospheric plasma waves; atmospheric and ionospheric physics, density and composition of the upper atmosphere, remote sensing using atmospheric radiation; solar physics, infrared astronomy, infrared signature analysis; infrared surveillance, imaging and remote sensing; multispectral and hyperspectral sensor development; data analysis and algorithm development; applications of multispectral and hyperspectral imagery to defense, civil space, commercial, and environmental missions; effects of solar activity, magnetic storms and nuclear explosions on the Earth's atmosphere, ionosphere and magnetosphere; effects of electromagnetic and particulate radiations on space systems; space instrumentation, design, fabrication and test; environmental chemistry, trace detection; atmospheric chemical reactions, atmospheric optics, light scattering, state-specific chemical reactions, and radiative signatures of missile plumes.